Effect of an axial pre-load on the flexural vibrations of viscoelastic beams

Elena Pierro

Abstract

Polymers are ultra-versatile materials that adapt to a myriad of applications, as they can be designed appropriately for specific needs. The realization of new compounds, however, requires the appropriate experimental characterizations, also from the mechanical point of view, which is typically carried out by analyzing the vibrations of beams, but which still have some unclear aspects, with respect to the well-known dynamics of elastic beams. To address this shortcoming, the paper deals with the theoretical modeling of a viscoelastic beam dynamics and pursues the elucidation of underlying how the flexural vibrations may be affected when an axial pre-load, compressive or tensile, is applied. The analytical model presented is able to shed light on a peculiar behavior, which is strongly related to the frequency-dependent damping induced by viscoelasticity. By considering as an example a real polymer, that is, a synthetic rubber, it is disclosed that an axial pre-load, in certain conditions, may enhance or suppress the oscillatory counterpart of a resonance peak of the beam, depending on both the frequency distribution of the complex modulus and the length of the beam. The analytical model is assessed by a finite element model, and it turns out to be an essential tool for understanding the dynamics of viscoelastic beams, typically exploited to experimentally characterize polymeric materials, and which could vary enormously simply through the application of constraints and ensued pre-loads.

1. Introduction

The new forthcoming technology challenges seem to be oriented toward the use of ultralight, extremely resistant, active, and super smart materials, substantially able to face with increasingly innovative shapes (Chaudhary et al., 2021), demands for adaptative features based on operating conditions (Terwagne et al., 2014), more in general with self-healing properties (Wang and Urban, 2020), and eco-sustainable (Ahmed, 2021). Of particular interest, more recently, are all those systems that aim to exploit the properties of soft materials, taking inspiration from biological systems, which offer countless performances, but that are also complex and therefore difficult to replicate. For example, soft actuators (Li et al., 2022) received great attention, since they can improve their performance through appropriate programming, and find applicability in the field of soft robotics (Cianchetti et al., 2018), which seem to show excellent results in terms of durability and reliability in the biomedical applications, and can transit reversibly between different liquids and solids, as they switch between different locomotive modes (Hu et al., 2018). These latest research trends are also part of the recently introduced concept of physical intelligence, which in the near future will allow intelligent machines to be able to move autonomously in various conditions of the real world (Sitti, 2021). As we move toward these scenarios, already widely present in our daily life in a vast range of applications, from the automotive to the medical field, it will no longer be possible to use materials "fixed" in their nominal design conditions, as they will need to be replaced by materials in constant movement and change (Martins, 2021; Rothemund et al., 2021).

1.1. The role of polymers

At the moment, polymers are between the favored materials and best suited to these circumstances, since they can be designed to serve a specific purpose, with properly tuned physical properties (Brinson and Brinson, 2015), such as

School of Engineering, University of Basilicata, Potenza, Italy

Corresponding author:
Elena Pierro, School of Engineering, University of Basilicata, Via dell'Ateneo Lucano, 10, Potenza 85100, Italy.
Email: elena.pierro@unibas.it

stiffness and damping. For this reason, they are the subject of intensive study in many engineering fields, especially for what regards their mechanical properties, which are deeply conditioned by viscoelasticity, as recently shown in the field of contact mechanics (Carbone and Pierro, 2012a, 2012b, 2013; Carbone et al., 2011). In Ref. Pierro et al. (2020), it has been highlighted that, in particular, the viscoelastic modulus, which exhibits a complex behavior in the frequency domain, is capable of making the adhesion between two surfaces extremely tough or quite weak, depending on how the imaginary part of the viscoelastic modulus is distributed in frequency. Whether polymers are employed individually or combined with other materials (e.g., in the case of composites), it is of fundamental importance to suitably characterize them from a mechanical point of view (Wang et al., 2017), for all the aforementioned applications. In fact, numerical and theoretical predictions of the dynamics rather than the tribological behavior of structures made of such materials are based on their viscoelastic response to external stresses, which depends on both frequency and temperature, and is governed by the following stress–strain relationship (Christensen, 1982)

$$\sigma(x, t) = \int\limits_{-\infty}^{t} G(t - \tau)\, \dot{\varepsilon}(x, \tau)\, \mathbf{d}\tau \qquad (1)$$

where $\dot{\varepsilon}(t)$ is the time derivative of the strain, $\sigma(t)$ is the stress, and $G(t - \tau)$ is the time-dependent relaxation function, usually characterized in the Laplace domain, through the viscoelastic modulus $E(s) = sG(s)$.

1.2. Viscoelastic modulus characterization

It is therefore quite evident that when polymers are employed, it is extremely important to know in detail the viscoelastic modulus and its trend as a function of both time and frequency. For this purpose, there is an awesome quantity of research devoted to the experimental characterization of this quantity, from the widespread dynamic mechanical analysis (DMA) technique (Rasa, 2014), which still presents some problems and uncertainties, to the investigation of the dynamics of beam-like structures (Caracciolo et al., 2004; Cortes and Elejabarrieta, 2007). In the context of this latter experimental approach, some progress has recently been made, as in Ref. Pierro and Carbone (2021), where the vibrational response of a suspended beam impacted with a hammer has been exploited to retrieve the complex modulus, increasing the frequency range of interest by varying the length of the beam. The technique is reliable, accurate, and in good agreement with the DMA. The breakthrough of the proposed technique is related to the analytical model presented, which is able to accurately take into account, in the vibrational response of the beam, the correct frequency trend of the viscoelastic modulus, by varying the number of relaxation times to achieve a good

theoretical–experimental fit. However, previous theoretical studies, focused on the dynamics of viscoelastic beam and plates (Garcia-Barruetabeña et al., 2012; Gupta and Khanna, 2007; Inman, 1989), lacked a specific analysis capable of linking the eigenvalues and the significant physical parameters to the analytical response of such continuous systems, as done, for example, in Ref. Adhikari (2005), for a single-degree-of-freedom non-viscously damped oscillator. To address this shortcoming, in Ref. Pierro (2020), some new characteristic maps related to the nature of the eigenvalues of a viscoelastic beam have been presented, with the aim to elucidate the influence of the material properties and of some geometrical characteristics on the overall beam dynamics. Interestingly, from this study, it resulted that by properly selecting the beam length, for a chosen viscoelastic material, it is possible to suppress or enhance one resonance peak or more peaks simultaneously. This outcome is of crucial concern for the experimental characterizations of viscoelastic materials, as the one presented in Pierro and Carbone (2021), since it can help in accurately interpreting the resonances when shifted with different beam lengths.

1.3. Contribute of the presented research

Even if the experimental technique for the viscoelastic modulus characterization based on beams appears to be promising for its simplicity, easy realization, and accuracy, it is necessary to understand how it is possible to increase the frequency range of analysis, still limited in comparison to the one of the DMA. Certainly, the variation of the length of the beam proposed in Pierro and Carbone (2021) already meets this requirement, thanks to the shift in frequency of the response and of the resonance peaks, but it is not yet completely exhaustive. Among the several possibilities to observe a further shift of the response spectrum of the beam in the frequency domain, and therefore to enlarge the frequency range of interest in the experimental characterization of the viscoelastic modulus, one may (i) change the surrounding temperature or (ii) apply an axial compressive/tractive pre-load to the beam. It is known (Cheli and Diana, 2015), indeed, that when an elastic beam is subjected to a static pre-load, its resonances move toward higher or lower frequencies, in case of an applied traction or compression, respectively. Many studies have been also carried out which investigate the effects of some dynamical axial pre-loads on both the flexural (Shih and Yeh, 2005) and the axial (Ebrahimi-Mamaghani et al., 2021) responses of the viscoelastic beams. However, to the author's knowledge, there are no specific studies in the literature that analyze how the transversal response of the viscoelastic beam changes in frequency because of static axial actions, with particular reference to the possible enhancement or suppression of one or more resonances. Controlling or even suppressing one or more resonance peaks in beam-like structures, indeed, is becoming an increasingly attractive research topic, especially in the very recent context of meta-materials (Hua et al., 2021; Zhang et al., 2022), for which it

is still necessary to continue studying several aspects, such as the contribution of the viscoelasticity of the polymeric materials typically employed. Starting from the previously presented theoretical study (Pierro, 2020) on the viscoelastic beams, the main motivation of this paper is therefore to get new insights on the nature of the eigenvalues, and consequently of the resonance peaks, when a tractive and a compressive pre-load are applied. A viscoelastic material with two relaxation times is considered, since it is always possible to divide the frequency spectrum under analysis in several intervals, thus allowing to decrease the number of the predominant relaxation times in such intervals (Figure 8 in Ref. Pierro (2019)). The results presented are validated by means of a finite element model (FEM) analysis and represent a step forward for the in-depth knowledge of polymeric materials, for the purpose of the possible control of their dynamic response, as well as to provide a useful tool to increase the frequency range in the experimental characterizations of the mechanical properties based on beams.

The paper is organized as follows: (i) in section 2, the dynamic response of the viscoelastic beam is obtained, including the presence of an axial static load; (ii) in section 3, the eigenvalues of the beam are calculated, and the dynamic response is written as a function of the eigenvalues; and (iii) in section 4, the results of both the analytical and the numerical models are shown, and a discussion on the impact of these results in the context of polymer research is presented.

2. Flexural vibrations of the tensioned beam

In this section, the analytical formulation to derive the equations which governs the flexural vibrations of an axially pre-loaded viscoelastic beam is presented. For this scope, a homogenous beam with rectangular cross section is considered (Figure 1(a)), where L is the length of the beam, and W and H are the width and the thickness of the beam cross section, respectively, which are supposed to follow the slenderness condition, that is, $L \gg W$ and $L \gg H$. Moreover, it is assumed that the beam always undergoes bending in a plane of symmetry and that the sections perpendicular to the axis remain plane during the motion. Since the study presented in this paper will be centered on the first resonances of the beam, which are not influenced by the shear deformations, the Bernoulli theory of transversal vibrations is exploited to describe the beam dynamics. This choice entails that the small displacements condition along the z-axis, that is, $|u(x, t)| \ll L$, needs to be satisfied.

The beam is supposed to be simply supported on both extremities, with an axial pre-load P applied at $x = L$ (Figure 1(b)). It is possible to prove, through simple calculations (see, for example, Ref. Cheli and Diana (2015), Section 3.3.1), that the effect of the static axial action P is introduced in the general equation of motion by means of the term $P \partial^2 u(x, t)/\partial x^2$. In the case of a beam with viscoelastic properties, the equation of motion is therefore (Inman, 1996; Pierro, 2020)

$$J_{xz} \int_{-\infty}^{t} E(t - \tau) \frac{\partial^4 u(x, \tau)}{\partial x^4} \, \mathbf{d}\tau + \mu \frac{\partial^2 u(x, t)}{\partial t^2} - P \frac{\partial^2 u(x, t)}{\partial x^2}$$
$$= f(x, t) \tag{2}$$

where $\mu = \rho A$, ρ is the bulk density of the material, $A = WH$ is the cross section area, $J_{xz} = (1/12)WH^3$ is the moment of inertia, and $f(x, t)$ is the generic forcing term. Any other damping terms may be added to equation (2) (Banks and Inman, 1991), such as the viscous and the hysteretic ones, but the presented analysis is only focused on the damping effect that comes from viscoelasticity. In order to solve equation (2), the associated homogeneous problem is firstly considered

$$J_{xz} \int_{-\infty}^{t} E(t - \tau) u_{xxxx}(x, \tau) \, \mathbf{d}\tau + \mu u_{tt}(x, t) - P u_{xx}(x, t) = 0 \tag{3}$$

together with the boundary conditions of the simply supported beam (Figure 1(b))

$$\begin{aligned} u(0, t) &= 0 \\ u_{xx}(0, t) &= 0 \\ u(L, t) &= 0 \\ u_{xx}(L, t) &= 0 \end{aligned} \tag{4}$$

having posed $u_x(x, t) = \partial u(x, t)/\partial x$, $u_t(x, t) = \partial u(x, t)/\partial t$. The solution of equation (3) can be easily found in the Laplace domain, with initial conditions equal to zero, so that the eigenfunctions $\phi(x, s)$ can be calculated solving the equation

$$\phi_{xxxx}(x) - P_{eq}\phi_{xx}(x) - \beta_{eq}^4(s)\,\phi(x) = 0 \tag{5}$$

with the boundary conditions

$$\begin{aligned} \phi(0) &= 0 \\ \phi_{xx}(0) &= 0 \\ \phi(L) &= 0 \\ \phi_{xx}(L) &= 0 \end{aligned} \tag{6}$$

having defined

$$\beta_{eq}^4(s) = -\frac{\mu s^2}{J_{xz}E(s)} \tag{7}$$

$$P_{eq} = \frac{P}{J_{xz}E(s)} \tag{8}$$

From the characteristic equation associated to equation (5)

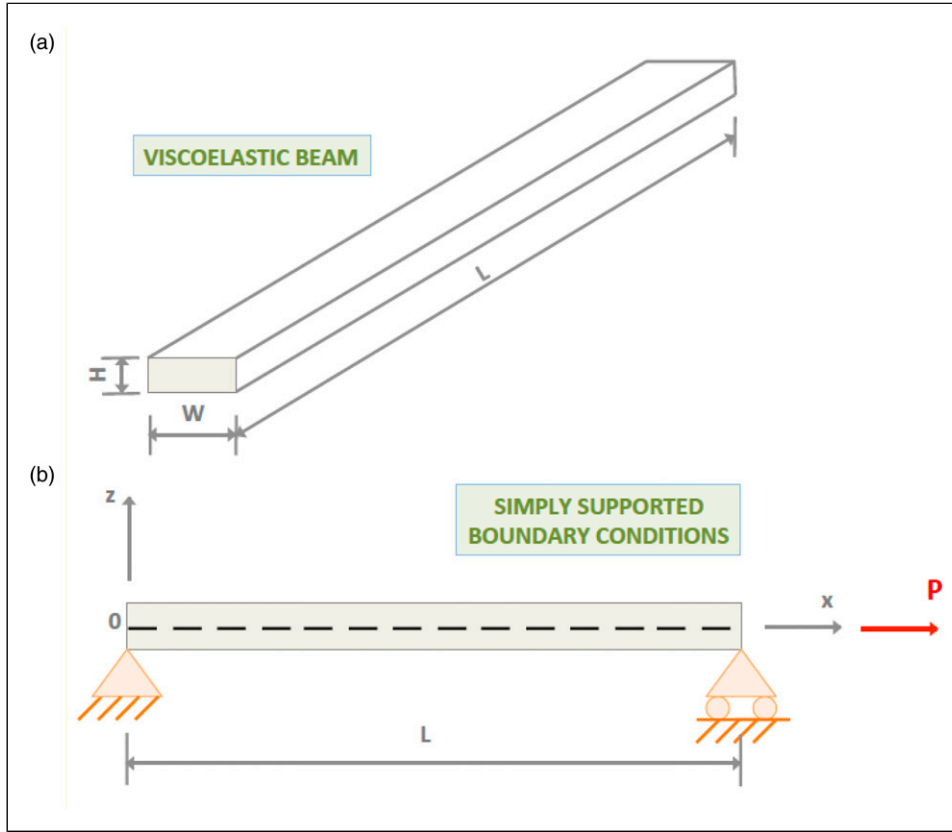$$\lambda^4(x) - P_{eq}\lambda^2(x) - \beta_{eq}^4(s) = 0 \tag{9}$$

Figure 1. The viscoelastic beam under investigation, of length L and rectangular cross section with area $A = WH$ (a), which is simply supported at both the extremities and axially pre-loaded (b).

one obtains the roots

$$\lambda_a^2 = \frac{P_{eq} - \sqrt{P_{eq}^2 + 4\beta_{eq}^4(s)}}{2}$$

$$\lambda_b^2 = \frac{P_{eq} + \sqrt{P_{eq}^2 + 4\beta_{eq}^4(s)}}{2}$$ (10)

from which

$$\lambda_{1,2} = \pm\sqrt{\lambda_a^2}$$

$$\lambda_{3,4} = \pm\sqrt{\lambda_b^2}$$ (11)

Finally, the solution of equation (5) can be written as

$$\phi(x, s) = W_1\sin[\gamma_1 x] + W_2\cos[\gamma_1 x] + W_3\sinh[\gamma_2 x] + W_4\cosh[\gamma_2 x]$$ (12)

where

$$\gamma_1 = \sqrt{-\lambda_a^2}$$

$$\gamma_2 = \sqrt{\lambda_b^2}$$ (13)

By forcing to zero the determinant of the system matrix obtained from equation (6), one has the equation

$$\sin(\gamma_1 L) = 0$$ (14)

which gives us same solutions $\gamma_{1_n}L = n\pi$ (Inman, 1996) of the elastic case. By substituting $\gamma_1^2 = -\lambda_a^2 = n\pi/L$ in equation (9), the following equation can be derived

$$\left(\frac{n\pi}{L}\right)^2 + P_{eq}\frac{n\pi}{L} - \beta_{eq}^4(s) = 0$$ (15)

from which it is possible to calculate the complex conjugate eigenvalues s_n corresponding to the n_{th} mode and the real poles s_k related to the material viscoelasticity (Pierro, 2020). Furthermore, the values γ_{1n} allow to determine the eigenfunctions $\phi_n(x)$

$$\phi_n(x) = \sin(\gamma_{1n}x)$$ (16)

that can be employed to get the general solution of equation (2), through the decomposition (Inman, 1989)

$$u(x, t) = \sum_{n=1}^{+\infty} \phi_n(x)\, q_n(t)$$ (17)

By following the same calculations shown in Ref. Pierro (2020), and by observing that

$$\phi_{n_{xx}}(x) = -\gamma_{1n}^2 \sin[\gamma_1 x] = -\gamma_{1n}^2 \phi_n(x)$$
$$\phi_{n_{xxxx}}(x) = \gamma_{1n}^4 \sin[\gamma_1 x] = \gamma_{1n}^4 \phi_n(x) \qquad (18)$$

it is straightforward to derive the projected equation of motion on the function $\phi_m(x)$ of the basis

$$\mu \ddot{q}_n(t) + J_{xz}\gamma_{1n}^4 \int\limits_{-\infty}^{t} E(t-\tau)\, q_n(\tau)\, \mathbf{d}\tau + \gamma_{1n}^2 P q_n(t) = f_n(t) \qquad (19)$$

where $f_n(t) = \frac{1}{L}\int_0^L f(x,\,t)\,\phi_n(x)\,\mathbf{d}x$ is the projected forcing term. By considering the Laplace transform of equation (19), with initial conditions equal to zero, and forcing term equal to the Dirac delta of constant amplitude F_0, in both the time and the spatial domains (i.e., $f(x,\,t) = F_0\delta(x-x_f)\,\delta(t-t_0)$), it is possible to obtain the system response

$$U(x,\,s) = F_0 \sum_{n=1}^{+\infty} \frac{\phi_n(x)\,\phi_n(x_f)}{\mu s^2 + \gamma_{1n}^2 P + J_{xz}\gamma_{1n}^4 E(s)} \qquad (20)$$

which clearly depends on the axial pre-load P.

3. Viscoelastic model—system eigenvalues

In order to determine the most important parameters which affect the system dynamics, some non-dimensional quantities will be defined. For this purpose, the general natural frequency of the transverse motions of a narrow, homogenous beam with a bending stiffness $E_0 J_{xz}$ and density ρ is considered

$$\omega_n = \left(\frac{c_n}{L}\right)^2 \sqrt{\frac{E_0 J_{xz}}{\rho A}} \qquad (21)$$

It should be noticed that equation (21) is always valid, regardless of the boundary conditions (Thomson and Dahleh, 1997), whereas the coefficient c_n depends on the specific boundary conditions. In particular, the first natural frequency is $\omega_1 = \alpha^2 \delta_1$, where $\delta_1 = c_1^2 \sqrt{E_0 A/(\rho J_{xz})}$, and $\alpha = R_g/L$ is the dimensionless beam length, with $R_g = \sqrt{J_{xz}/A}$ being the radius of gyration. In the case of a rectangular beam cross section, one has $\alpha = H/(\sqrt{12}\,L)$ and $\delta_1 = (c_1^2/H)\sqrt{12 E_0/\rho}$. It is so possible to define the non-dimensional eigenvalue $\bar{s} = s/\delta_1$, and in particular one has, for the n_{th} mode, $\omega_n^2 = E_0\beta_n^4 J_{xz}/\mu = r_n E_0$ and $\delta_n = c_n^2\sqrt{E_0 A/(\rho J_{xz})}$, where $r_n = (\beta_n)^4 J_{xz}/\mu$.

Among the several constitutive models available in literature, generally exploited to describe the stress–strain relation in equation (1), in this study, the generalized Maxwell model is utilized, which considers a spring and k Maxwell elements connected in parallel. The viscoelastic modulus $E(s)$ in the Laplace domain, in particular, is represented by the following discrete function

$$E(s) = E_0 + \sum_k E_k \frac{s\tau_k}{1+s\tau_k} \qquad (22)$$

where E_0 is the elastic modulus of the material at zero-frequency, and τ_k and E_k are the relaxation time and the elastic modulus, respectively, of the generic spring-element in the generalized linear viscoelastic model (Christensen, 1982). The number of relaxation times τ_k typically required to well convey the complex modulus in a wide frequency range can be of the order of a few tens. However, it has been recently shown that (Pierro, 2019, 2020; Pierro and Carbone, 2021), in a narrow frequency range, for example, around a resonance peak, even just two relaxation times are adequate for a very good representation of the modulus in that specific range. Since the present study focuses on the analysis of some first peaks, considered individually, and since the system is linear, the viscoelastic modulus will be represented just through two relaxation times τ_1 and τ_2. The corresponding complex function equation (22), with $k = 2$, can be therefore substituted in equation (15), and the fourth-order characteristic equation, for each n_{th} mode, can be written

$$\bar{s}^4 + \sum_{j=0}^{3} a_j \bar{s}^j = 0 \qquad (23)$$

where

$$a_0 = \alpha^4 \Delta_n^2 \frac{1}{\theta_1 \theta_2} + \frac{\alpha^2 \Delta_n \overline{P}}{\theta_1 \theta_2}$$

$$a_1 = \left(\frac{1}{\theta_2} + \frac{1}{\theta_1} + \frac{\gamma_1}{\theta_2} + \frac{\gamma_2}{\theta_1}\right)\alpha^4 \Delta_n^2 + \frac{\alpha^2 \Delta_n \overline{P}}{\theta_2} + \frac{\alpha^2 \Delta_n \overline{P}}{\theta_1}$$

$$a_2 = \left(\frac{1}{\theta_1 \theta_2} + \alpha^4 \Delta_n^2 + \alpha^4 \Delta_n^2 \gamma_1 + \alpha^4 \Delta_n^2 \gamma_2\right) + \alpha^2 \Delta_n \overline{P}$$

$$a_3 = \left(\frac{1}{\theta_1} + \frac{1}{\theta_2}\right) \qquad (24)$$

having defined the non-dimensional axial pre-load $\overline{P} = P/(c_1^2 E_0 A)$, the non-dimensional groups $\gamma_1 = E_1/E_0$, $\gamma_2 = E_2/E_0$, $\theta_1 = \delta_1 \tau_1$, $\theta_2 = \tau_2 \delta_1$, and being $\Delta_n = \delta_n/\delta_1$. For the quartic equation (23), the following discriminant $D(n)$ (Lazard, 1988; Rees, 1922) can be defined

$$D(n) = 256a_0^3 - 192a_3 a_1 a_0^2 - 128a_2^2 a_0^2 + 144a_2 a_1^2 a_0 - 27a_1^4 + 144a_3^2 a_2 a_0^2 - 6a_3^2 a_1^2 a_0 - 80a_3 a_2^2 a_1 a_0$$
$$+ 18a_3 a_2 a_1^3 + 16a_2^4 a_0 - 4a_2^3 a_1^2 - 27a_3^4 a_0^2 + 18a_3^3 a_2 a_1 a_0 - 4a_3^3 a_1^3 - 4a_3^2 a_2^3 a_0 + a_3^2 a_2^2 a_1^2 \qquad (25)$$

which plays a fundamental role in the general dynamics of the beam, since it influences the nature of the roots of equation (23). Two of the four roots, in particular, are always real and are related to an overdamped motion. The other two roots can be (i) complex conjugate, representing the oscillatory contribute to the n_{th} mode in the beam dynamics, or (ii) both real, meaning that the n_{th} mode is not oscillatory. Finally, the acceleration of a generic beam cross section $A(x, \overline{s}) = \overline{s}^2 U(x, \overline{s})$ can be written as a function of the non-dimensional parameters defined above

$$A\left(x, \overline{s}\right) = F_0 \sum_{n=1}^{+\infty} \frac{\overline{s}^2 \left(1 + \theta_1 \overline{s}\right) \left(1 + \theta_2 \overline{s}\right) \varphi_n(x) \, \varphi_n\left(x_f\right)}{\mu \theta_1 \theta_2 \left(\overline{s}^4 + \sum_{j=0}^{3} a_j \overline{s}^j\right)}$$

(26)

4. Results

The main results deriving from the theoretical analysis presented in this paper will be shown below. For the scope, the viscoelastic beam considered in Figure 1 is studied when oscillating in the xz-plane, having a rectangular cross section with fixed thickness $H = 1$[cm]. The beam length L is considered varying by means of the parameter $\alpha = R_g/L$, keeping $R_g = H/\sqrt{12}$ constant. Regarding the material of the beam, it should be observed that the investigation here presented focuses the attention on the peculiarity of polymers to be "materials in continuous change," meaning that they see the elastic constants E_k and the relaxation times τ_k deeply changing under some operational conditions, for example, with the environmental temperature. In this perspective, a sensitive study, based on a fully characterized self-adhesive synthetic rubber (Ref. Rouleau et al. (2015), has been carried out, by varying the aforementioned constants. The elastic modulus has been pretty well fitted by means of equation (2) in Pierro (2020) (which here corresponds to equation (22)), with two relaxation times, in the frequency range $0 - 10$[rad/s]. In this range, in particolar, it is possible to oberve the first resonance of a beam made of this material and with length $\tilde{L} = 50$[cm], that is, $\tilde{\alpha} = R_g/\tilde{L} = 0.0058$, here considered as reference. The parameters obtained from the fitting procedure are shown in Table 1, where $\delta_1 = 72*10^3$ for the considered boundary conditions.

In order to evaluate the effect of an axial pre-load applied to the beam, on the first flexural mode ($n = 1$), the nature of the four roots of equation (23) is analyzed by plotting in Figure 2 the discriminant $D(1)$ (equation (25)) as a region map, obtained by varying the parameter values $(\alpha, \overline{P})$, for $\theta_1 = \overline{\theta}_1$, $\theta_2 = \overline{\theta}_2$, $\gamma_1 = \overline{\gamma}_1$, and $\gamma_2 = \overline{\gamma}_2$.

In the areas where $D(1)$ is positive, the first peak is suppressed, but it is clear that, for the considered geometry

Table 1. Viscoelastic parameters of a self-adhesive rubber (Rouleau et al., 2015), obtained by the fitting procedure shown in Ref. Pierro (2020).

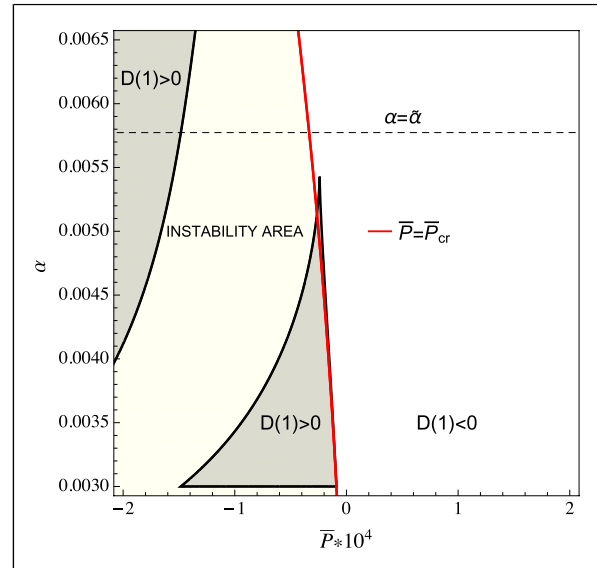| Viscoelastic constants	
$E_0 = 4.46*10^5$	[Pa]
$E_1 = 3.25*10^6$	[Pa]
$E_2 = 1.63*10^5$	[Pa]
$\tau_1 = 0.0314$	[s]
$\tau_2 = 0.314$	[s]
$\overline{\gamma}_1 = E_1/E_0 = 7.287$	
$\overline{\gamma}_2 = E_2/E_0 = 0.36547$	
$\overline{\theta}_1 = \delta_1 \tau_1 = 2260.8$	
$\overline{\theta}_2 = \delta_1 \tau_2 = 22608$	

Figure 2. The region map for the first natural frequency $n = 1$, for $\theta_1 = \overline{\theta}_1$, $\theta_2 = \overline{\theta}_2$, $\gamma_1 = \overline{\gamma}_1$, and $\gamma_2 = \overline{\gamma}_2$. For $D(1) > 0$, the first peak is suppressed. No tensile loads determine such condition, while for compressive loads, the shaded areas are almost on the left of the static Euler's critical loads calculated for every value of α (red solid line), which is the area of instability.

($\alpha = \tilde{\alpha}$) and material, there is no tensile load which determines such condition. Even if some shaded areas with $D(1) > 0$ exist for compressive pre-loads, they are not worthy of attention, as they correspond to loads greater than Euler's critical load $P_{cr} = -E_0 J_{xz} \pi^2/L^2$ (Timoshenko and Gere, 1961), which is plotted in the non-dimensional form $\overline{P}_{cr}(\alpha) = P_{cr}/(c_1^2 E_0 A)$ in Figure 2 (red curve), as a function of the parameter α, thus delimiting the region of instability (yellow shaded area). Having a map of this type allows us to understand, therefore, if the application of an axial pre-load can in some way enhance or reduce the dynamic response of the beam, at a certain resonant frequency, as will be shown later.

It is now interesting to understand if any variation of the viscoelastic modulus, due to (i) a change in the composition of the internal material compound or (ii) a surrounding temperature variation, with a consequent shift of the complex modulus in the frequency domain, may somehow affect the nature of the roots, for one or more resonance peaks. The first condition is studied by considering, for example, the change of the constant E_1, that is, by varying the parameter γ_1, as shown in Figure 3, where the viscoelastic modulus $E(\omega)$ is plotted, in terms of the real part $\text{Re}[E(\omega)]$ (Figure 3(a)) and the function $\tan\delta = \text{Im}[E(\omega)]/\text{Re}[E(\omega)]$ (Figure 3(b)), for different values of γ_1.

It is possible to observe that by increasing γ_1, both the real part and the damping contribute, represented by the function $\tan\delta$, tend to increase. The influence of the working temperature change, which determines a frequency shift of both the real part and the imaginary part of the complex modulus $E(\omega)$, is analyzed by varying the first relaxation time τ_1, that is, by changing the parameter $\overline{\theta}_1$. In Figure 4, in fact, one can see that an increase of θ_1 just determines a shift of both the real part $\text{Re}[E(\omega)]$ (Figure 4(a)) and the function $\tan\delta$ (Figure 4(b)), toward lower frequencies, without affecting the amount of both the damping, represented by the function $\tan\delta$ and the real part of the complex modulus.

Focusing the attention again on the first flexural mode ($n = 1$), the region map of the discriminant $D(1)$ is plotted in Figure 5(a), for the same numerical values used in Figure 2, except for γ_1, which is now considered equal to $\gamma_1 = 5\overline{\gamma}_1$.

It is clear that in this case, the shaded areas, corresponding to the condition $D(1) > 0$, hence to the first peak suppression, regard also the positive tractive loads. This circumstance can be better highlighted by representing the system response in two points, A and B, for $\alpha = \tilde{\alpha}$, without pre-tension $\overline{P} = 0$ (point A) and for a tractive pre-load $\overline{P} = 2*10^{-4}$ (point B). In Figure 5(b), the
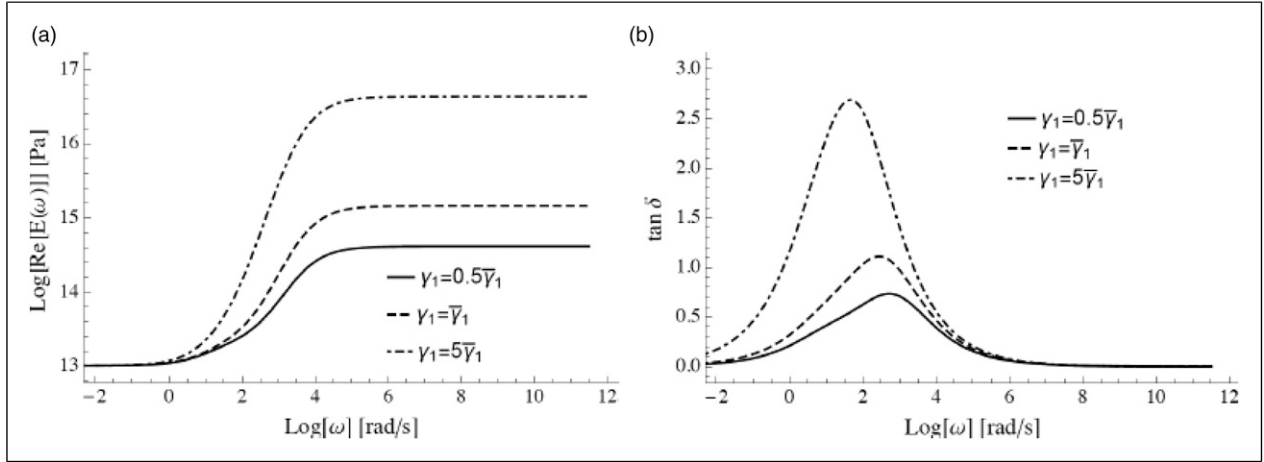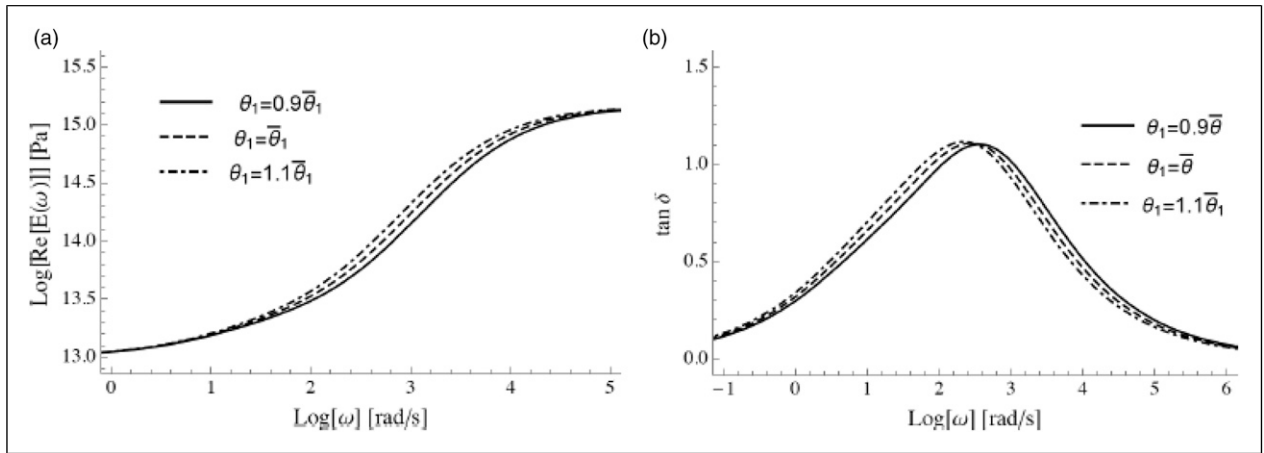

Figure 3. The viscoelastic modulus $E(\omega)$, as real part $\text{Re}[E(\omega)]$ (a), and the function $\tan\delta$ (b), for $\theta_1 = \overline{\theta}_1$, $\theta_2 = \overline{\theta}_2$, and $\gamma_2 = \overline{\gamma}_2$, and for $\gamma_1 = 0.5\overline{\gamma}_1$ (solid lines), $\gamma_1 = \overline{\gamma}_1$ (dashed lines), and $\gamma_1 = 5\overline{\gamma}_1$ (dot dashed lines).

Figure 4. The viscoelastic modulus $E(\omega)$, as real part $\text{Re}[E(\omega)]$ (a), and the function $\tan\delta$ (b), for $\theta_2 = \overline{\theta}_2$, $\gamma_1 = \overline{\gamma}_1$, and $\gamma_2 = \overline{\gamma}_2$, and for $\theta_1 = 0.9\overline{\theta}_1$ (solid lines), $\theta_1 = \overline{\theta}_1$ (dashed lines), and $\theta_1 = 1.1\overline{\theta}_1$ (dot dashed lines).
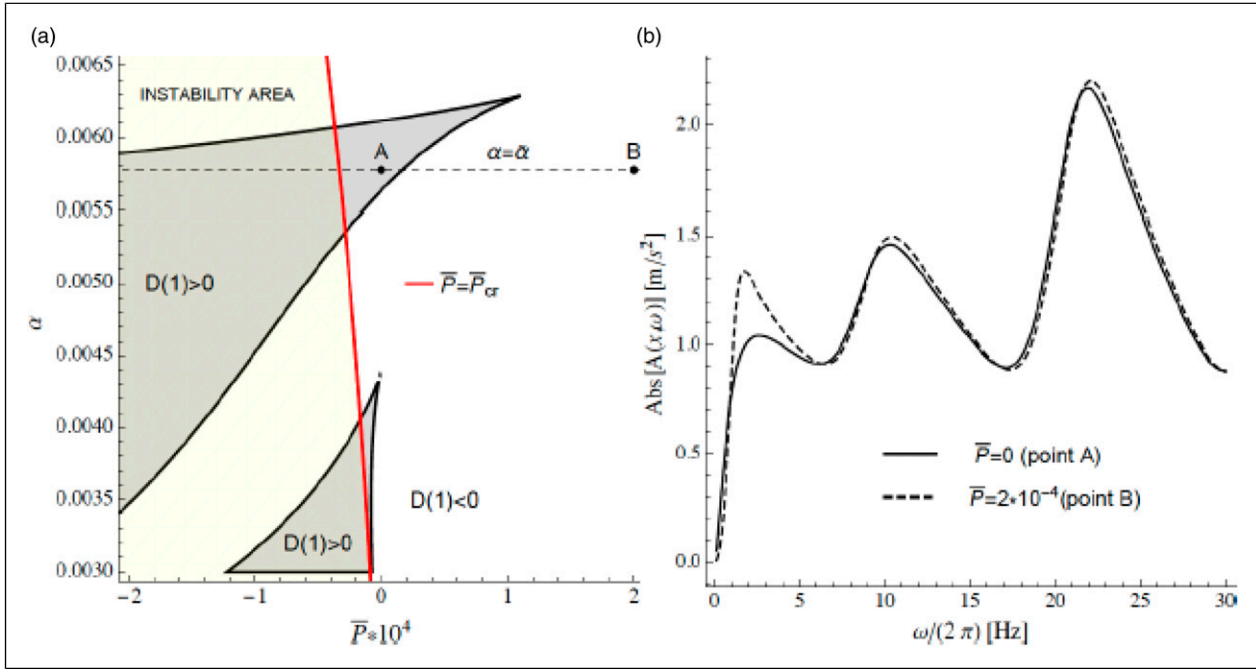
Figure 5. The region map corresponding to the first natural frequency $n = 1$, for $\theta_1 = \bar{\theta}_1$, $\theta_2 = \bar{\theta}_2$, $\gamma_1 = 5\bar{\gamma}_1$, and $\gamma_2 = \bar{\gamma}_2$. The discriminant is positive for tractive pre-loads (e.g., point B), while the peak suppression may occur in absence of pre-loads (e.g., point A). The static Euler's critical load is represented (red solid line) (a). The acceleration modulus $|A(\bar{x}, \omega)|$ is plotted in frequency for $\bar{P} = 0$ (point A) and $\bar{P} = 2*10^{-4}$ (point B) (b).

acceleration modulus $|A(\bar{x}, \omega)|$ (equation (26)), evaluated at the beam section $x = x_f = \bar{x} = 0.4\tilde{L}$, and for $\theta_1 = \bar{\theta}_1$, $\theta_2 = \bar{\theta}_2$, $\gamma_1 = 5\bar{\gamma}_1$, and $\gamma_2 = \bar{\gamma}_2$, is shown for the two points of Figure 5(a), A and B. It is quite clear that the beam presents a first mode suppression, when no axial load is applied (point A, black solid line). However, when the beam is pre-loaded through a tensile load $\bar{P} = 2*10^{-4}$ (point B, black dashed line), which corresponds to a force $P \cong 1[\text{N}]$, the first mode becomes again oscillatory, and a peak close to $10[\text{rad/s}]$ is well visible. These results highlight the usefulness of the proposed maps, which make it possible to predict whether the response of the beam can be amplified or reduced, simply by applying a slight axial pre-load. The practical implications of this result fall within the contexts of the experimental characterization of viscoelastic materials, that is, where the absence of a peak can lead to misinterpreting the nature of the material itself, or more in general where systems made of beams are pre-loaded, and the impact of this action on the dynamic response should be suitably predicted.

To better understand the influence of the parameters γ_1 and θ_1 on the nature of the system roots, and in particular the behavior of the viscoelastic beam at its first natural frequency, the discriminant $D(1)$ is shown as a function of the pre-tension $\bar{P}$, at the fixed beam length $\alpha = \tilde{\alpha}$, for different values of γ_1 (Figure 6) and θ_1 (Figure 7).

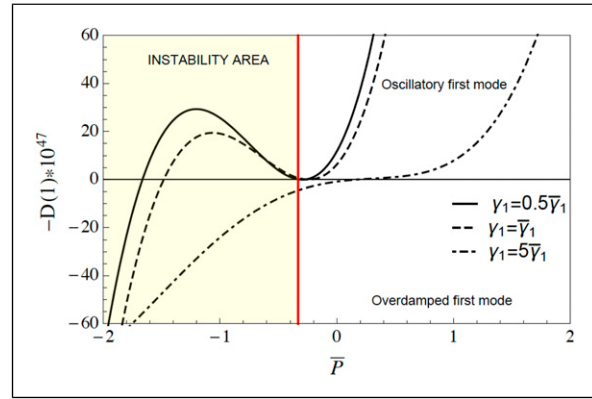For the particular case considered, in terms of geometrical and material properties, and hence beam length, it

Figure 6. The discriminant $D(1)$ as a function of the non-dimensional pre-load $\bar{P}$, for $\alpha = \tilde{\alpha}$, $\theta_1 = \bar{\theta}_1$, $\theta_2 = \bar{\theta}_2$, and $\gamma_2 = \bar{\gamma}_2$, and for different values of γ_1, that is, $\gamma_1 = 0.5\bar{\gamma}_1$ (solid line), $\gamma_1 = \bar{\gamma}_1$ (dashed line), and $\gamma_1 = 5\bar{\gamma}_1$ (dot dashed line). The red line corresponds to Euler's critical load.

is quite evident in Figure 6, again, that an increase of γ_1, that is, for $\gamma_1 = 5\bar{\gamma}_1$, the first resonance is also suppressed in absence of pre-load, and that tensile pre-loads could rehabilitate the oscillatory motion of the beam at its first natural frequency. On the contrary, the motion is always oscillatory for any variation of θ_1, as shown in Figure 7, except for slight compressive loads, up to Euler's critical load $\bar{P}_{cr}(\alpha = \tilde{\alpha}) \cong -0.33$.

As a consequence of what is shown in Figures 6 and 7, it is important to understand that a certain viscoelastic system, such as the beam under examination, can undergo a drastic variation in its dynamics, through the simultaneous action of an axial pre-load and a variation of the viscoelastic properties of the material of which the system is made. These variations, in particular, can be related to a change in the working temperature, a very frequent circumstance in 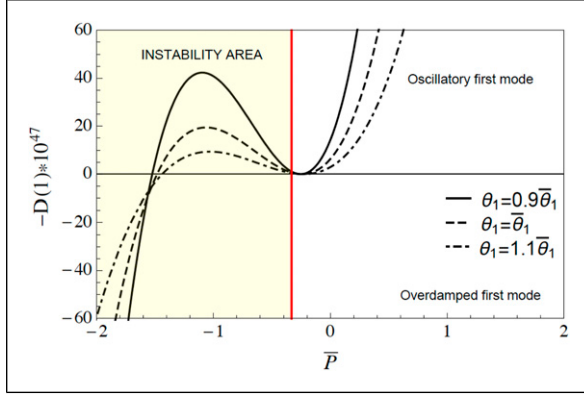all those systems made of polymeric materials, subject to significant thermal excursions during their operational conditions (e.g., wind turbines (Tefera et al., 2022)).

5. Finite element model simulation and final remarks

The beam under investigation, of length $\tilde{L} = 50$[cm], that is, $\tilde{\alpha} = 0.0058$, and material properties reported in Table 1, has been modeled in Abaqus (2018) by means of 6400 solid linear hexahedron element type (C3D8). The boundary conditions have been applied at the two extremities, at the middle plane of the beam, to simulate the simply supported BC. A constant force in the frequency domain, with unit amplitude, has been applied at the beam section $x_f = 0.4\tilde{L}$, where the beam acceleration has been calculated ($x = x_f = 0.4\tilde{L}$), through the steady-state dynamics module. In Figure 8, the acceleration modulus $|A(\bar{x}, \omega)|$ is plotted near the first natural frequency, for $\theta_1 = \bar{\theta}_1$, $\theta_2 = \bar{\theta}_2$, $\gamma_1 = \bar{\gamma}_1$, and $\gamma_2 = \bar{\gamma}_2$, when no static pre-load is applied (Figure 8(a)), and in presence of a tractive pre-load $\bar{P} = 2*10^{-4}$ (Figure 8(b)), for both the models, numerical (solid lines) and analytical (dashed lines).

The agreement between the two models is well established, and the considerable increase of the acceleration amplitude due to the application of a tensile load (Figure 8(b)) is quite congruent with the region map shown in Figure 2, which foresees a low peak in the absence of pre-load, because we are close to the area with a positive discriminant $D(1) > 0$. In the case of applied pre-load, on the
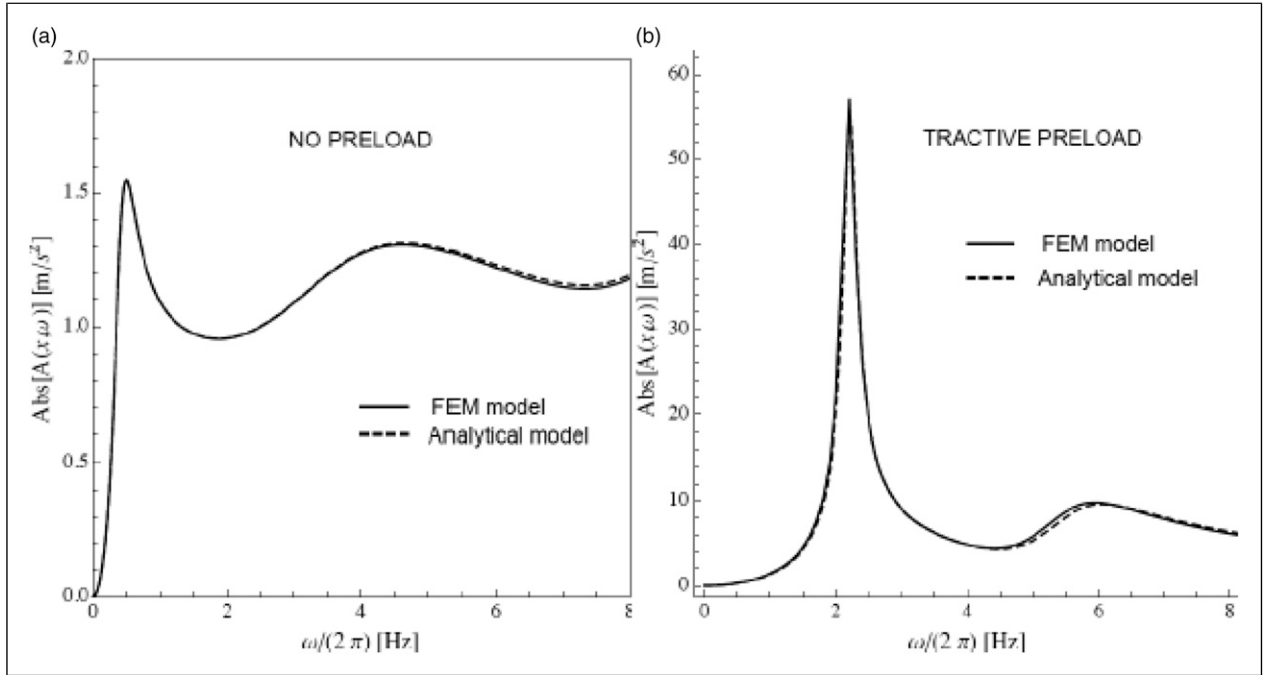
Figure 7. The discriminant $D(1)$ as a function of the non-dimensional pre-load $\bar{P}$, for $\alpha = \tilde{\alpha}$, $\theta_2 = \bar{\theta}_2$, $\gamma_1 = \bar{\gamma}_1$, and $\gamma_2 = \bar{\gamma}_2$, and for $\theta_1 = 0.9\bar{\theta}_1$ (solid line), $\theta_1 = \bar{\theta}_1$ (dashed line), and $\theta_1 = 1.1\bar{\theta}_1$ (dot dashed line). The red line corresponds to Euler's critical load.

Figure 8. The acceleration modulus $|A(\bar{x}, \omega)|$, in the section $x = x_f = 0.4\tilde{L}$, for $\bar{P} = 0$ (a) and for $\bar{P} = 2*10^{-4}$ (b). In both the cases, a good agreement has been achieved, between the FEM analysis (solid lines) and the theoretical model (dashed lines).
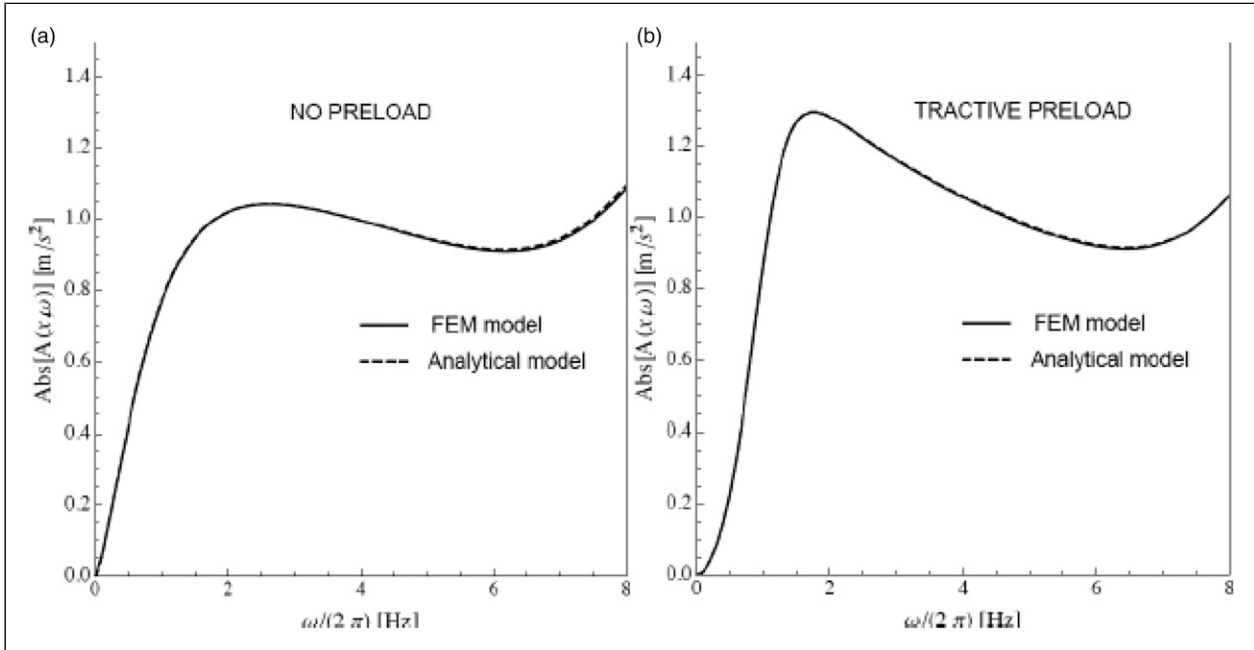
Figure 9. The acceleration modulus $|A(\bar{x}, \omega)|$, in the section $x = x_f = 0.4\tilde{L}$, this time with $\gamma_1 = 5\bar{\gamma}_1$, for $\bar{P} = 0$ (a) and for $\bar{P} = 2*10^{-4}$ (b). Also in this case, it is possible to ascertain the good agreement between the FEM analysis (solid lines) and the theoretical model (dashed lines).

other hand, we are very far from the area of the oscillatory motion suppression, and the peak is particularly enhanced. Furthermore, in Figure 9, the acceleration modulus $|A(\bar{x}, \omega)|$ is shown for the same beam and the same material, except for the parameter γ_1, which is now taken $\gamma_1 = 5\bar{\gamma}_1$. For both the cases, that is, in absence of pre-load (Figure 9(a)) and in presence of a static tension $\bar{P} = 2*10^{-4}$ (Figure 9(b)), the results coming from the theoretical model presented in this paper follow pretty well the curves obtained by the FEM analysis, and the reduced amplitude of the first peak is again in agreement with what has been argued about Figure 5. Therefore, the comparison between the analytical model and the numerical one, the latter based on solid elements, that is, of a completely different nature (not as the 1D Euler–Bernoulli beam elements), has produced perfectly consistent results and definitively confirms the accuracy of the analytical model here presented.

In conclusion, through the proposed analytical model, which now takes into account the presence of a static pre-load acting on the viscoelastic beam, it is possible to fully evaluate the dynamic response of this kind of system, which strongly differs from the case of a perfectly elastic beam, because of viscoelasticity. The enhancement or the suppression of a resonance peak, which occurs only by slightly varying an axial pre-load and that, in particular conditions, can also be involuntary and due to the effective application of the constraints in the experimental activities, is strategic in the context of the characterization

of such materials. In the most popular classical techniques, such as the DMA, the accurate positioning of the constraints on the beam can be decisive in order to retrieve the correct viscoelastic constants. Furthermore, in the more recently proposed experimental method (Pierro and Carbone, 2021), where the resonance peaks are moved in the frequency spectrum by changing the beam length, with the aim to increase the range of interest under investigation, the controlled application of an axial pre-load may be strategic to further increase the width of the frequency range. Finally, the study here presented discloses aspects on polymers not highlighted so far, which further position them among the most versatile and tunable materials, crucial for all current and future applications.

6. Conclusions

In this work, an analytical model has been proposed which is able to accurately describe the transversal dynamics of viscoelastic beams, also taking into account the effect of axial pre-loads. The main purpose is to evaluate how these pre-loads determine a variation of the nature of the system's eigenvalues, and therefore on the type of vibrational motion of the beam at a certain resonance frequency. Because of the viscoelasticity, and the related damping distribution on frequency, the behavior of the beam is not as simple and predictable as in the case of perfectly elastic beams. By applying a tensile or a compressive axial pre-load, one may

observe the enhancement or the mitigation of a resonance peak, but this circumstance is incidental to a pivotal geometrical parameter, that is, the beam length. Same observations have been made through an FEM analysis, which has provided results perfectly in agreement with those obtained from the analytical model. This theoretical model has made it possible to get new insights on how the mechanical characteristics of polymers can completely change the dynamic behavior of a beam. On one hand, these findings are essential for all experimental applications that make use of beams to characterize the complex viscoelastic module, and on the other, they further point out the versatility of polymers and how they increasingly reflect the perfect peculiarities that are required by the materials of the future.

Declaration of conflicting interests

Funding

ORCID iD

Elena Pierro ⓘ https://orcid.org/0000-0002-3056-0290

References

Abaqus (2018) *Abaqus Documentation*. Providence, RI: Dassault Systèmes.

Adhikari S (2005) Qualitative dynamic characteristics of a non-viscously damped oscillator. *Proceedings of the Royal Society A: Mathematical, Physical & Engineering Sciences* 461(2059): 2269–2288.

Ahmed S (2021) *Advanced Green Materials Fabrication, Characterization and Applications of Biopolymers and Biocomposites*. Duxford: Woodhead Publishing in Materials.

Banks HT and Inman DJ (1991) On damping mechanisms in beams. *Journal of Applied Mechanics* 58(3): 716–723.

Brinson HF and Brinson LC (2015) Characteristics, applications and properties of polymers. In: *Polymer Engineering Science and Viscoelasticity*. Boston, MA: Springer.

Caracciolo R, Gasparetto A and Giovagnoni M (2004) An experimental technique for complete dynamic characterization of a viscoelastic material. *Journal of Sound and Vibration* 272(35): 1013–1032.

Carbone G and Pierro E (2012a) Sticky bio-inspired micropillars: finding the best shape. *Small* 8(9): 1449–1454.

Carbone G and Pierro E (2012b) Effect of interfacial air entrapment on the adhesion of bio-inspired mushroom-shaped micropillars. *Soft Matter* 8(30): 7904–7908.

Carbone G and Pierro E (2013) A review of adhesion mechanisms of mushroom-shaped microstructured adhesives. *Meccanica* 48(8): 1819–1833.

Carbone G, Pierro E and Gorb S (2011) Origin of the superior adhesive performance of mushroom shaped microstructured surfaces. *Soft Matter* 7(12): 5545–5552.

Chaudhary G, Prasath SG, Soucy E, et al. (2021) Totimorphic assemblies from neutrally stable units. *Proceedings of the National Academy of Sciences* 118(42): e2107003118.

Cheli F and Diana G (2015) *Advanced Dynamics of Mechanical Systems*. Cham: Springer Verlag.

Christensen RM (1982) *Theory of Viscoelasticity*. NY: Academic Press.

Cianchetti M, Laschi C, Menciassi A, et al. (2018) Biomedical applications of soft robotics. *Nature Reviews Materials* 3: 143–153.

Cortes F and Elejabarrieta MJ (2007) Viscoelastic materials characterisation using the seismic response. *Materials and Design* 28(7): 2054–2062.

Ebrahimi-Mamaghani A, Forooghi A, Sarparast H, et al. (2021) Vibration of viscoelastic axially graded beams with simultaneous axial and spinning motions under an axial load. *Applied Mathematical Modelling* 90: 131–150.

García-Barruetabeña J, Cortés F and Abete JM (2012) Dynamics of an exponentially damped solid rod: analytic solution and finite element formulations. *International Journal of Solids and Structures* 49(3–4): 590–598.

Gupta AK and Khanna A (2007) Vibration of visco-elastic rectangular plate with linearly thickness variations in both directions. *Journal of Sound and Vibration* 301(3–5): 450–457.

Hu W, Lum G, Mastrangeli M, et al. (2018) Small-scale soft-bodied robot with multimodal locomotion. *Nature* 554: 81–85.

Hua G, Austin ACM, Sorokin V, et al. (2021) Metamaterial beam with graded local resonators for broadband vibration suppression. *Mechanical Systems and Signal Processing* 146: 106982.

Inman DJ (1989) Vibration analysis of viscoelastic beams by separation of variables and modal analysis. *Mechanics Research Communications* 16(4): 213–218.

Inman DJ (1996) *Engineering Vibrations*. Upper Saddle River, NJ: Prentice Hall.

Lazard D (1988) Quantifier elimination: optimal solution for two classical examples. *Journal of Symbolic Computation* 5(1–2): 261–266.

Li M, Pal A, Aghakhani A, et al. (2022) Soft actuators for real-world applications. *Nature Reviews Materials* 7: 235–249.

Martins R (2021) Materials as activator of future global science and technology challenges. *Progress in Natural Science: Materials International* 31(6): 785–791.

Park SW and Schapery RA (1999) Methods of interconversion between linear viscoelastic material functions. Part I-A

numerical method based on Prony series. *International Journal of Solids and Structures* 36(11): 1653–1675.

Pierro E (2019) Viscoelastic beam dynamics: theoretical analysis on damping mechanisms. In: *7th International Conference on Computational Methods in Structural Dynamics and Earthquake Engineering*, Crete, Greece, 24 June 2019, pp.4396–4407.

Pierro E (2020) Damping control in viscoelastic beam dynamics. *Journal of Vibration and Control* 26(19–20): 1753–1764.

Pierro E and Carbone G (2021) A new technique for the characterization of viscoelastic materials: theory, experiments and comparison with DMA. *Journal of Sound and Vibration* 515: 116462.

Pierro E, Afferrante L and Carbone G (2020) On the peeling of elastic tapes from viscoelastic substrates: designing materials for ultratough peeling. *Tribology International* 146: 106060.

Rasa A (2014) Applying dynamic mechanical analysis to research and development for viscoelastic damping materials. In: *Internoise 2014*, Melbourne, Australia, 16–19 November 2014. Magill: Australian Acoustical Society.

Rees EL (1922) Graphical discussion of the roots of a quartic equation. *The American Mathematical Monthly* 29(2): 51–55.

Rothemund P, Kim Y, Heisser RH, et al. (2021) Shaping the future of robotics through materials innovation. *Nature Materials* 20(12): 1582–1587.

Rouleau L, Pirk R, Pluymers B, et al. (2015) Characterization and modeling of the viscoelastic behavior of a self-adhesive rubber using dynamic mechanical analysis tests. *Journal of Aerospace Technology and Management* 7(2): 200–208.

Shih and Yeh (2005) Dynamic stability of a viscoelastic beam with frequency-dependent modulus. *International Journal of Solids and Structures* 42(7): 2145–2159.

Sitti M (2021) Physical intelligence as a new paradigm. *Extreme Mechanics Letters* 46: 101340.

Tefera G, Adali S and Bright G (2022) Flexural and viscoelastic properties of FRP composite laminates under higher temperatures: experiments and model assessment. *Polymers* 14(11): 2296.

Terwagne D, Brojan M and Reis PM (2014) Smart morphable surfaces for aerodynamic drag control. *Advanced Materials* 26(38): 6608–6611.

Thomson WT and Dahleh MD (1997) *Theory of Vibration with Applications*. 5th edition. Englewood Cliffs, NJ: Prentice Hall.

Timoshenko SP and Gere JM (1961) *Theory of Elastic Stability*. NY: McGraw-Hill.

Wang S and Urban MW (2020) Self-healing polymers. *Nature Reviews Materials* 5: 562–583.

Wang Y, Zhu C, Pfattner R, et al. (2017) A highly stretchable, transparent, and conductive polymer. *Science Advances* 3(3): e1602076.

Zhang J, Zhang X, Zhang H, et al. (2022) Rainbow zigzag metamaterial beams as broadband vibration isolators for beam-like structures. *Journal of Sound and Vibration* 530: 116945.

Appendix 1

Nomenclature

List of symbols

A	cross section area
$A(x, \omega)$	acceleration of the beam in the frequency domain
$D(n)$	discriminant of the n_{th}-mode
E	viscoelastic modulus
f	force acting on the beam
G	relaxation function
H	thickness of the beam cross section
J_{xz}	moment of inertia
L	length of the beam
n	mode of vibration
P	axial pre-load
R_g	radius of gyration
s	Laplace domain variable
t	time domain variable
$u(x, t)$	displacements along the z-axis (time domain)
$U(x, s)$	displacements along the z-axis (Laplace domain)
W	width of the beam cross section
x	spatial domain variable
α	dimensionless beam length
γ_k	non-dimensional group related to E_k
$\delta(t)$	Dirac delta function
ε	strain
θ_k	non-dimensional group related to τ_k
λ	root of the characteristic equation
ρ	bulk density
σ	stress
τ	relaxation time
φ	system eigenfunctions
ω	angular frequency
$\cdot_x(x, t) = \partial \cdot (x, t)/\partial x$	spatial derivative
$\cdot_t(x, t) = \partial \cdot (x, t)/\partial t$	time derivative
$\lvert \cdot \rvert$	modulus

Subscripts

f	stands for force location
cr	denotes the Euler's critical load
$k = 1...n$	denotes the number of relaxation time
$th = 1...n$	number of mode of vibration